Structural and Luminescence Properties of Transparent Nanocrystalline ZrO_2:Er^{3+} Films *

ZHANG Qin-Yuan(张勤远)[1**], YANG Gang-Feng(杨钢锋)[1], JIANG Zhong-Hong(姜中宏)[1], W. X. Que[2]

[1]*Key Laboratory of Specially Functional Materials of Ministry of Education and Institute of Optical Communication Materials, South China University of Technology, Guangzhou 510640*

[2]*School of Materials Science and Engineering, Nanyang Technological University, Nanyang Avenue, Singapore 639798, Singapore*

(Received 7 December 2005)

The structural and luminescence properties of nanocrystalline ZrO_2:Er^{3+} films are reported. Transparent nano-ZrO_2 crystalline films doped with Er^{3+} have been prepared using a wet chemistry process. An intense room-temperature emission at 1527 nm with a full width at half-maximum of 46 nm has been observed, which is assigned to the $^4I_{13/2} \rightarrow {}^4I_{15/2}$ intra-$4f^n$ electric transition of Er^{3+}. Correlations between the luminescence properties and structures of the nanocrystalline ZrO_2:Er^{3+} films have been investigated. Infrared-to-visible upconversion occurs simultaneously upon excitation of a commercially available 980-nm laser diode and the involved mechanisms have also been explained. The results indicate that the nanocrystalline ZrO_2:Er^{3+} films might be suggested as promising materials for achieving broadband Er^{3+}-doped waveguide amplifiers and upconversion waveguide lasers.

PACS: 42. 70. − a, 68. 55. Jk, 78. 55. − m, 78. 20. − e

Following the demonstration of a high-gain, low-noise optical amplifier at 1.5 μm, which is in agreement with the third communication window, by using a single-mode silica fibre, there has been a reawakening of interest in trivalent erbium ions-doped materials, and a surge of activity on silica fibre amplifiers has therefore followed.[1] Recently, erbium-doped materials via the sol-gel chemistry process have been recognized to hold tremendous potential in the area of photonic applications.[2−7] The as-synthesized sol-gel products can be conveniently converted into thin film configurations, powder, bulk solid and fibres to meet different applications of our modern day needs. Especially, with the advent of the sophistication of advanced microfabrication facilities and new material technologies, diffractive and miniaturized optical gratings have widely been used in optical systems. The simplicity of the sol-gel chemistry device fabrication process and the possibility of ultraviolet (UV) patternable behaviours of the sol-gel materials could certainly suggest that the sol-gel materials are more promising and important for low-cost and mass production of integrated photonic circuits.[8]

ZrO_2 has attracted a great deal of attention for potentially optical applications over the past several years because of its superior hardness, high refractive index, optical transparency, and photothermal stability.[9] It has been used in waveguides, interferometry, and coating for high power laser mirrors.[10−12] Furthermore, the stretching frequency of ZrO_2 is at around 470 cm^{-1}. This low phonon energy opens up a possibility of higher efficient luminescence of active ions incorporated into ZrO_2 matrix. Some of these applications are considered to be waveguide amplifiers, new generation television screens, solid-state white light sources and biomedical diagnostics.[10−12] Nanocrystalline ZrO_2, on the other hand, has recently been demonstrated to present suitable optical properties for their photonic applications due to its enhanced luminescence properties,[10−12] which in turn is due to nano-size effects. Considering the promising optical properties of nanocrystalline ZrO_2:Er^{3+} and the simplicity of the sol-gel chemistry device fabrication process, it is interesting to evaluate the luminescence and Infrared-to-visible upconversion of transparent nanocrystalline ZrO_2:Er^{3+} films. In this Letter, we present our study on the preparation and characterization of nanocrystalline ZrO_2:Er^{3+} films obtained by a hydrothermal synthesis and a sol-gel chemistry process. It should be mentioned that the advantages of this method over the other methods are the good control on the structure and refractive index of nanocrystalline ZrO_2:Er^{3+} films and also the ability to purify the precursors for high-purity products. By using the present method, it has been possible to synthesize high-quality nanocrystalline ZrO_2:Er^{3+} films with large amounts of Er^{3+}, and the nano-ZrO_2 material can be made into a waveguide with a large index difference between the guiding and the cladding region, thus providing a strong mode confinement, which is suitable for rare-earth doped lasers and amplifiers.

ZrO_2 films doped with 2 mol% Er_2O_3 were pre-

* Supported by the National Natural Science Foundation of China under Grant No 50472053, NCET (NCET04-0823) and DSTG (04020036 and 2004A10602002).

** To whom correspondence should be addressed. Email: qyzhang@scut.edu.cn

©2006 Chinese Physical Society and IOP Publishing Ltd

pared by a hydrothermal synthesis and a sol-gel chemistry process. In brief, an Er^{3+}-doped aqueous solution of $ZrOCl_2$ was prepared firstly using zirconium oxychloride octahydrate ($ZrOCl_2{\cdot}8H_2O$, 99.0%) and erbium chloride ($ErCl_3$). The hydrolysis reaction could be given as $ErCl_3 + ZrOCl_2 + (n+1)H_2O \rightarrow [ZrO_2 \cdot nH_2O]{:}Er^{3+} + 2HCl + 3Cl^-$. The pH value of the solution was less than 1.0. In order to absorb and remove the hydrochloric acid produced, a basic amine-formaldehyde resin was added. The obtained clear solution was then held in a stainless steel autoclave with a Teflon liner at 450°C for 1 h, and it was subsequently quenched in an ice-bath to room temperature (RT). Finally, the water was replaced by methoxyethanol (b.p.124°C) through the distillation process. A clear, stable, and ethanolic $ZrO_2{:}Er^{3+}$ sol was deposited on quartz and/or silicon wafer by employing a spin-coating technique at 2500 rpm for 30 s in a controlled N_2 atmosphere. The $ZrO_2{:}Er^{3+}$ films were densified by annealing at temperatures from 500 to 700°C for about 10 min using a rapid thermal process in N_2 atmosphere.

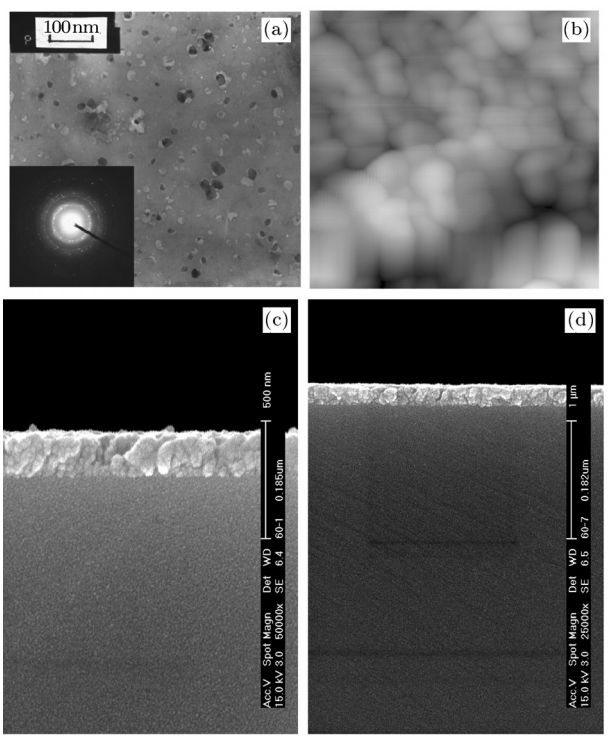


Fig. 1. TEM image of as-prepared clear ethanolic $ZrO_2{:}Er^{3+}$ sol with SAED pattern (a), the SPM image of the surface of nanocrystalline $ZrO_2{:}Er^{3+}$ films obtained after annealed at 700°C (b), the cross-section FE-HRSEM micrograph of nanocrystalline $ZrO_2{:}Er^{3+}$ films obtained after annealed at 500°C (c) and 700°C (d).

Transmission electron microscopy (TEM) (Model JEM-200CX) was used to characterize the synthesized ethanolic $ZrO_2{:}Er^{3+}$ sol, as shown in Figs. 1(1)–1(d). Figure 1(a) presents the TEM image of the as-prepared clear ethanolic $ZrO_2{:}Er^{3+}$ sol. The size of the $ZrO_2{:}Er^{3+}$ nanoparticles was found to rang from 10 to 20 nm in diameter. A selected-area electron diffraction (SAED) pattern of the ZrO_2 nanoparticles was also carried out. This SAED pattern gives clear crystal diffraction rings as shown in the inset of Fig. 1(a), indicating that the $ZrO_2{:}Er^{3+}$ nanoparticles have already been a crystalline structure. Figure 1(c) illustrates a cross-section image of the deposited $ZrO_2{:}Er^{3+}$ films that were annealed at 500°C, obtained by a field emission high-resolution scanning electron microscope (FE-HRSEM) (Model XL30 FEG, Philips Corp.), and the result indicates that the nanocrystalline $ZrO_2{:}Er^{3+}$ films have varied sizes ranging from 40 to 60 nm and the thickness of the films was about 185 nm. It should be noted that the nanocrystalline $ZrO_2{:}Er^{3+}$ films have become densified with the firing temperature increase. The refractive index was measured on a Metricon 2010 by means of the prism coupling technique. A 0.8-mW He-Ne laser tube with standard silicon detectors was employed to operate at 0.633 μm. The refractive index of the nanocrystalline $ZrO_2{:}Er^{3+}$ films was found to be 1.55 at 633 nm as deposited, and increased to 1.59 and 1.70 with an increase in the annealing temperature from RT to 500 and 700°C, respectively. The porosity of the films could be calculated by $P = 1 - \dfrac{n^2-1}{n_0^2-1}$, where n is the refractive index of the porous films, and n_0 is the refractive index of pore-free ZrO_2 ($n_0 = 2.1$). It can be obtained that the porosity of the nano-ZrO_2 thin films has been decreased to 55.2% and 44.5% from 58.9% with an increase of annealing temperature from RT to 500 and 700°C, respectively. Meanwhile the film thickness has been decreased to 185 and 182 nm from 190 nm because of the densification of these films further. Well-crystallized $ZrO_2{:}Er^{3+}$ films with an average grain size of around 80 nm has clearly been noticed from SEM and a scanning probe microscope (SPM) image (obtained by a Digital Instruments-Dimension 3000) of the film annealed at 700°C as shown in Figs. 1(d) and 1(b).

To confirm further the aforementioned crystallization behaviour of the nanocrystalline $ZrO_2{:}Er^{3+}$ films, x-ray diffraction (XRD) analysis (Siemens-D5005 X-Ray Diffractometry, Cu K_α target with a working voltage of 40 kV and a current of 40 mA) has also been carried out and the XRD patterns are shown in Fig. 2. From these XRD patterns it might be detected the presence of both tetragonal (t-ZrO_2) and monoclinic (m-ZrO_2) phases of ZrO_2 according to the standard JCPDS 37-1413 and JCPDS 37-1484, respectively. It is evident from the results as presented in Fig. 2 that when the film is annealed at 500°C, the intensities of these XRD diffraction peaks are relatively weak, but the intensities of the XRD peaks increase with the increasing heat treatment temperature up to 700°C. It should be mentioned that no phases other

than ZrO_2 are detectable for the film with Er^{3+} contents up to 2 mol%. These XRD results clearly demonstrate that nanocrystalline ZrO_2:Er^{3+} films could be obtained with the annealing temperature of more than 500°C.

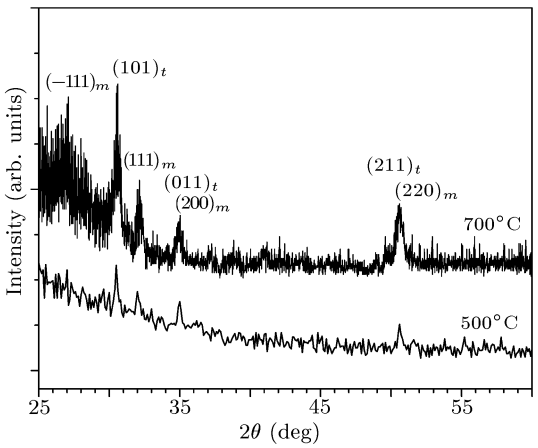


Fig. 2. XRD patterns of 2 mol% Er^{3+}-doped nanocrystalline ZrO_2 films obtained after annealing at different temperatures.

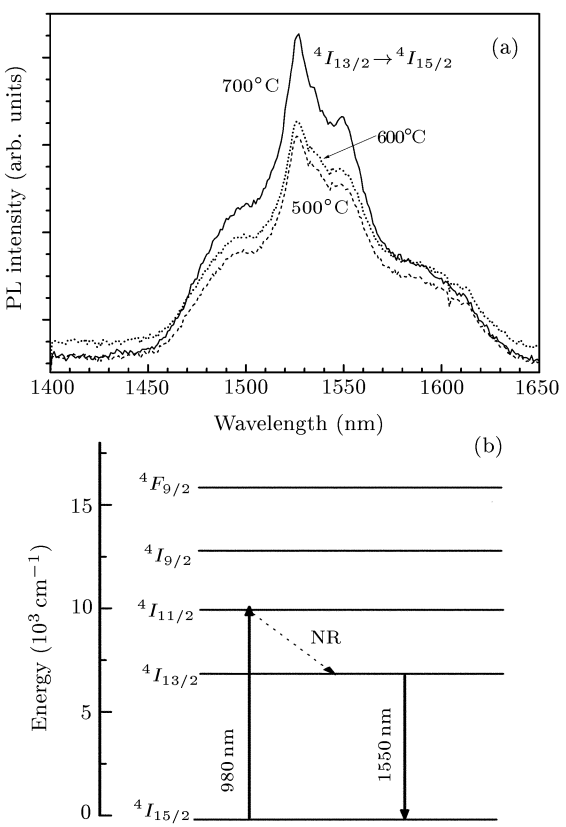


Fig. 3. (a) NIR emission spectra of nanocrystalline ZrO_2:Er^{3+} films obtained after annealing at different temperatures. (b) A partial energy level diagram indicating the $^4I_{13/2} \rightarrow {}^4I_{15/2}$ intra-$4f^n$ transition of Er^{3+}.

A computer-controlled Triax 320 spectrofluorimeter (Jobin-Yvon Co.) with a 980 nm laser diode (LD) was used for the photoluminescence (PL) characterization. Emitted light was focused onto the monochromator and was monitored at the exit slit by using a photon-counting R5108 photomultiplier tube (400–1200 nm) for the visible up-conversion emission and InGaAs detector (800–1650 nm) for 1.5-μm emission, and finally amplified with a Stanford SR830SP lock-in amplifier. Figure 3(a) shows the PL spectra of the nanocrystalline ZrO_2:Er^{3+} films annealed at different temperatures with an excitation at 980 nm LD. An intense RT 1.5-μm emission at 1527 nm and a full width at half-maximum (FWHM) of 46 nm, which corresponds to the $^4I_{13/2} \rightarrow {}^4I_{15/2}$ intra-$4f^n$ transition of Er^{3+} (as shown in Fig. 3(b)), has been measured and examined it as a function of the annealing temperature. It can be seen that the peak intensities slightly increase with the increasing annealing temperature. However, the peak position and the FWHM of the Er^{3+} emission have hardly been changed with the annealing temperatures. In particular, the shape, peak position and FWHM of our PL spectra have been found to be quite satisfactorily comparable with those prepared by other methods.[1,3,5,13]

IR-to-visible upconversion luminescence has simultaneously been excited using 980 nm LD with a pump of 1.5-μm emission, as shown in Fig. 4(a). Three emission bands centred at 524, 546 and 668 nm, which are assigned to the electronic transitions of $^2H_{11/2} \rightarrow {}^4I_{15/2}$, $^4S_{13/2} \rightarrow {}^4I_{15/2}$ and $^4F_{9/2} \rightarrow {}^4I_{15/2}$ of Er^{3+} ions, respectively, are clearly observed from these films. The possible upconversion mechanisms have been explained in terms of an energy level diagram of Er^{3+} as shown in Fig. 4(b).[14,15] Firstly, Er^{3+} ions in the ground state could be excited directly to the excited level $^4I_{11/2}$ upon LD pump and then these excited Er^{3+} ions would undergo different processes for green and red emissions. For the green emission, there are two possible upconversion mechanisms such as energy transfer (ET) and excited state absorption (ESA). When the concentration of Er^{3+} ions in the $^4I_{11/2}$ level is high enough, ET between two Er^{3+} ions takes place, i.e., an Er^{3+} ion transfers energy to the other and return the ground state, and simultaneously the acceptor ion goes to a higher energy level $^4I_{7/2}$: Er^{3+} ($^4I_{11/2}$) + Er^{3+} ($^4I_{11/2}$) $\rightarrow$ Er^{3+} ($^4F_{7/2}$) + Er^{3+} ($^4I_{15/2}$). ESA is also a main contribution to the green luminescence. An Er^{3+} ion in the excited state $^4I_{11/2}$ absorbs a pump photon again resulting in an excited $^4F_{15/2}$ level: Er^{3+} ($^4I_{11/2}$) +a photon $\rightarrow$ Er^{3+} ($^4F_{7/2}$) and hence the next lower $^4H_{11/2}$ and $^4S_{3/2}$ levels are populated by the excited state Er^{3+} ions of $^4F_{7/2}$ level relaxing nonradiatively due to the narrow energy gaps between them, about 1300 cm^{-1} from the absorption spectral data. The energy gap between the next energy level $^4F_{9/2}$ and the $^4S_{3/2}$ level is large, which is about 3200 cm^{-1}. The nonradiative transition from

the $^4S_{3/2}$ level becomes small, and the populations of the $^4S_{3/2}$ level are larger than that of the $^4H_{11/2}$ level. Therefore, the above processes could cause a weaker emission $^2H_{11/2} \rightarrow {}^4I_{15/2}$ at 524 nm and reveals a prominently intense green emission $^4S_{15/2} \rightarrow {}^4I_{15/2}$ at 546 nm. On the other hand, for the red upconversion, it corresponds to the process that the $^4I_{13/2}$ energy level is populated through a multiphonon relaxation of Er^{3+} ions in the excited state $^4I_{11/2}$. Then both the ESA and ET upconversion mechanisms could occur in the $^4I_{13/2}$ level. These processes have been described as Er^{3+} ($^4I_{13/2}$) + Er^{3+} ($^4I_{11/2}$) $\rightarrow$ Er^{3+} ($^4F_{9/2}$) + Er^{3+} ($^4I_{15/2}$), and Er^{3+} ($^4I_{13/2}$) +a photon $\rightarrow$ Er^{3+} ($^4F_{9/2}$), respectively. Another possible mechanism could be a nonradiative multiphonon decay from the $^4S_{3/2}$ level to the $^4F_{9/2}$ level. Based on the above-mentioned cause, this could be treated as a remote possibility. Since the green emission at 546 nm is stronger than red emission at 668 nm, there might be more populations on the $^4S_{3/2}$ level.

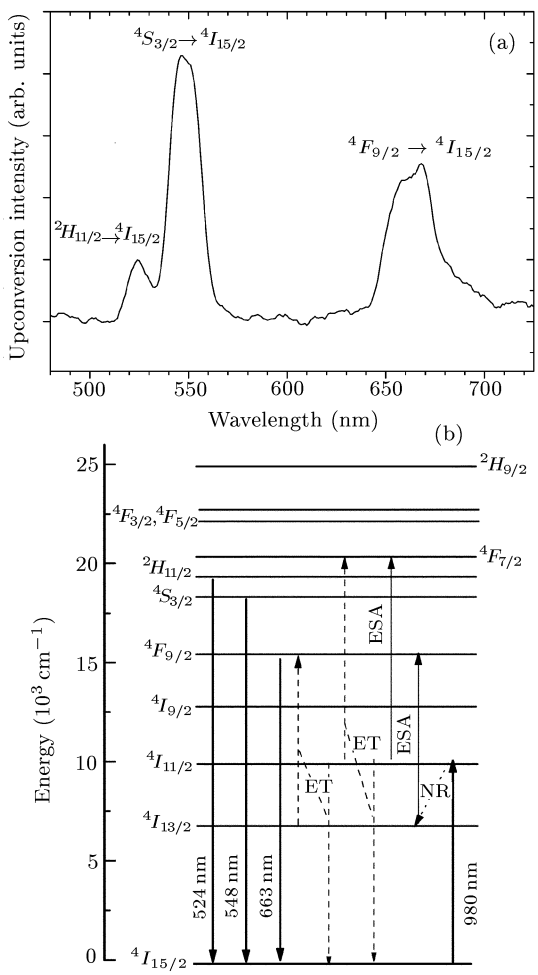


Fig. 4. (a) IR-to-visible upconversion emission spectrum of nanocrystalline ZrO_2:Er^{3+} films obtained after annealed at 700°C. (b) A schematic energy level diagram and up-conversion process of nanocrystalline ZrO_2:Er^{3+} films under infrared excitation.

In summary, transparent nano-ZrO_2 crystalline films with crystalline diameters of 40–60 nm and film thickness of 160–180 nm doped with Er^{3+} have been prepared using a hydrothermal synthesis and a sol-gel chemistry process. Both the optical and structural properties of these nanocrystalline ZrO_2:Er^{3+} films have been investigated. An intense room temperature 1.5-μm emission has been observed as a function of the annealing temperature. Infrared-to-visible upconversion occurs simultaneously upon excitation with a commercially available 980 nm LD. The results indicate that the rare-earth doped nanocrystalline ZrO_2:Er^{3+} films could be suggested as more promising materials to achieve broadband Er^{3+}-doped waveguide amplifiers and upconversion waveguide lasers.

References

[1] Digonnet M J F 2001 *Rare-Earth-Doped Fiber Lasers and Amplifiers* (New York: Dekker) p 96

[2] Que W X, Zhou Y, Lam Y L, Zhou J et al 2001 *J. Appl. Phys.* **89** 3058

[3] Benatsou M, Capoen B, Bouazaoui M et al 1997 *Appl. Phys. Lett.* **71** 428

[4] Orignac X, Barbier D, Du X M and Almeida R M 1996 *Appl. Phys. Lett.* **69** 895

[5] Ryu C K, Choi H and Kim K 1995 *Appl. Phys. Lett.* **66** 2496

[6] Bouazaoui M, Bahtat A and Garapon C et al 1996 *J. Non-Cryst. Solids* **202** 16

[7] Reisfeld R and Jorgensen C K 1992 *Structure and Bonding* (Berlin: Springer) vol 77 p 207

[8] Que W X, Hu X and Zhang Q Y 2003 *Chem. Phys. Lett.* **369** 354
Zhang Q Y, Pita K et al 2004 *Appl. Phys. Lett.* **84** 1638

[9] Harrison H D E, McLamed N T and Subbarao E C 1963 *J. Electrochem. Soc.* **110** 23

[10] Patra A, Friend C S, Kapoor R and Prasad P N 2003 *Appl. Phys. Lett.* **83** 284

[11] Rosa-Cruz E De la Diaz-Torres L A, Salas P et al 2003 *Appl. Phys. Lett.* **83** 4903

[12] Salas P, Angeles-Chavez C, Montoya J A et al 2005 *Opt. Mater.* **27** 1295

[13] Sun H T, Zhang L Y, Duan Z C et al 2005 *Chin. Phys. Lett.* **22** 1249
Zhang Q Y, Yang G F, Buddhudu S et al 2005 *Chin. Phys. Lett.* **22** 715

[14] Pollnau M, Gamelin D R, Luthi S R et al 2000 *Phys. Rev.* B **61** 3337

[15] Berthou H and Jorgensen C K 1990 *Opt. Lett.* **15** 1100